LUND UNIVERSITY

Master of Science Thesis

Using q-space Diffusion MRI for Structural Studies of a Biological Phantom at a 3T Clinical Scanner

Anna Rydhög

Supervisor: Sara Brockstedt, Jimmy Lätt

Medical Radiation Physics
Clinical Sciences, Lund

Lund University, 2007

Abstract

Diffusion magnetic resonance imaging (MRI) is today a well-established method in clinics around the world. For example it is a leading method for diagnosing ischaemic stroke at an early stage. Trough research it is a continuously growing field applicable to many different tasks.

Alternatively, the diffusion MRI can be used for morphologic studies by the use of q-space analysis. q-space imaging is an established method in NMR spectroscopy for retrieving structural information from biological materials. Structural q-space imaging at a clinical scanner is more difficult to achieve due to limited gradient performance, however apparent mean displacement data has been presented *in vivo*.

The aim of this study was to investigate the possibility for absolute quantification of fiber structure sizes in a biological phantom, using the full width at half maximum (FWHM) of the diffusion propagator and microscopy images were obtained as a "golden standard reference".

The results from the analysis made on *Asparagus officinalis* show, as expected, that water molecules diffuse like free water along the fibres, while the water diffusion perpendicular to the fibers is restricted. The sizes of these structures were obtained and agreed very well with the microscopy images.

Content

Introduction

Magnetic resonance imaging (MRI) is a method for visualizing the inside of, for example, the human body without using ionizing radiation, such as x-rays, or surgery. Instead it is magnetism and magnetic fields oscillating in the radio frequency domain that work together to produce valuable images.

Nuclear magnetic resonance (NMR), the phenomenon in which magnetic fields and radio waves cause protons (hydrogen atoms) to give off radio frequent signals, was first discovered in the 1930s by Felix Bloch and Edward Purcell. They used the NMR spectroscopy as a method for investigating chemical compounds. In 1970, Raymond Damadian constructed the first whole-body MRI scanner, the "indomitable". He also found that different kinds of animal tissues emit time varying response signals, a discovery which today is used for creating contrast in MRI. In 2003, Paul C Lauterbur and Sir Peter Mansfield were awarded the Nobel Prize in Physiology or Medicine for their discoveries concerning MRI and the groundwork of the magnetic resonance tomography (MRT).

One way to generate contrast in MRI is to use the diffusion properties of water molecules. Since Moseley *et al.* discovered the importance of diffusion weighted images (DWI) to diagnose acute ischaemic stroke in the early 1990s[1], the technique has continuously been improved. Today it is a valuable tool when examining patients with e.g. multiple sclerosis (MS), Alzheimer's disease and brain tumours.

Diffusion is a physical process, which can be described as a random walk of a particle. The mobility of the particle is characterized by a physical constant called the diffusion coefficient, *D*. Structures, such as cell walls and fibre bundles, which surround the particle, highly influences the mobility and causes a reduction of the apparent diffusion coefficient and that is why, *in vivo*, the apparent diffusion coefficient (ADC) is measured instead. The ADC can also be influenced by active processes such as within the studied tissue, and is thus a tool for understanding and diagnosing various disease processes or abnormal development.

In a pure liquid, the distance a particle diffuses is equal in all directions. This is called isotropic diffusion. When instead the travelled distance is different for different directions the diffusion is called anisotropic. The anisotropy is thus directly related to the geometry of the fibres.

In many of the early studies regarding anisotropy the ratio of ADC parallel and ADC perpendicular to different fibrous structures was measured[2]. Measurements of water diffusion in human brain was early performed by Thomsen *et al*. It was shown that white brain matter had regional differences in diffusion due to orientation of the myelin sheats. It was concluded that water molecules preferentially diffuse along the length of the axons and on the other hand is hindered by myelin sheets perpendicular to the axons.

If the diffusion time, i.e. the time we allow the molecules to move during the experiment, is so long that the water molecules are able to bounce against the cell walls, there is a possibility to calculate the cell size as the mean distance they have moved. It is done with what's called q-space imaging. When q-space imaging, first developed for NMR spectroscopy, now is introduced in the clinical environment, new ways of characterizing anisotropy has been found. The full width at half maximum (FWHM) of the diffusion propagator is one of the parameters, which come out of a q-space analysis, and is related to the mean displacement of the diffusing molecules. This leads to a way of deciding structural sizes much smaller than a conventional MR image can resolve.

Diffusion MRI is still a burgeoning field and the development in this area is strong. My contribution to the development has been to find a suitable phantom for anisotropic diffusion measurements. A further step has been to determine the confinement of the phantom's structure using a clinical scanner. This has so far only been performed by NMR spectrometers.

The implementation of this technique would be an important step towards further knowledge about the different water components, such as intra – and extra cellular, in the human brain and what we're really looking at. If we fully understood these different components contribution to the diffusion contrast, there is a possibility to also understand these components pathologic behaviour.

Aim of this study

The aim of this study was to find a suitable phantom for anisotropic diffusion and then to determine structural sizes by the use of the q-space method and validate it with measurements made on a microscopy.

Theory of Diffusion MRI

The diffusion process

Diffusion is a translational motion of molecules present in most materials, when temperatures are above 0˚ K, and it is driven by a thermally dependent random motion, called Brownian motion. Molecular weight, intermolecular interactions (viscosity) and temperature are important factors of which the diffusion process depends on.

The physical process of diffusion can be described by Fick's second law which states that for a constant diffusion coefficient, *D*, the rate of change in concentration, *C*, with time, t, is proportional to the rate at which the concentration gradient changes with distance, *x*, in a given direction. In the one-dimensional case Fick's law is written as

$$\frac{\partial C}{\partial t} = D\frac{\partial^2 C}{\partial^2 x} \qquad \textbf{eq. 1}$$

D is commonly given in m^2/s and is $2.13 \cdot 10^{-9}$ m^2/s for water[3] at a temperature of 20˚ C.

In the three dimensional case **eq. 1** can be extended to:

$$\frac{\partial C}{\partial t} = D\left(\frac{\partial^2 C}{\partial x^2} + \frac{\partial^2 C}{\partial y^2} + \frac{\partial^2 C}{\partial z^2}\right) = D\nabla^2 C \qquad \textbf{eq. 2}$$

which only holds for isotropic diffusion, i.e. when the diffusion is equivalent in all directions.

The diffusion that occurres when mixing two different liquids or gases are preferably described in terms of the concentration gradient of the diffusing substance, as seen above. The concentration gradient is however not the driving force of the random diffusion which is present in all materia. Instead the motion of water within water, driven by thermal agitation, is thought to be the important process. This process is commonly referred to as self-diffusion[4] and is described in terms of displacement probability. The probability is defined as *P(s,t)* where s is the relative dynamic displacement at the time *t*. In analogy with the equations above the self-diffusion can be described by

$$\frac{\partial P}{\partial t} = D\nabla^2 P \qquad \textbf{eq. 3}$$

At $t = 0$ the probability distribution is a delta function that spreads out to a Gaussian distribution as the time elapses.

Gaussian diffusion

The free self-diffusion is the random displacement of molecules in no preferred direction. It is described by a displacement probability distribution defined by $P(\bar{r}_0, \bar{r}_1, t)$. This self-correlation function describes the conditional probability of finding a particle initially at position $\bar{r}_0$, at a position $\bar{r}_1$ after a time t[5]. This probability distribution function is a delta function for $t = 0$, and as t is prolonged it extends to a Gaussian distribution. The mean square displacement for free self-diffusion can then be determined according to

$$\left\langle \left| \bar{r}_1 - \bar{r}_0 \right|^2 \right\rangle = 2n_d DT_D \qquad \textbf{eq. 4}$$

where n_d is the number of dimensions. For free diffusion, the mean square displacement increases linearly with the diffusion time. The diffusion coefficient for freely diffusing particles will therefore be independent of the diffusion time and the displacement in any arbitrary direction will reflect the true diffusion rate.

Motion sensitive encoding

If a spatially dependent magnetic field gradient is applied additionally to the B_0-field, the Larmor frequency, i.e. the angular velocity of the precession around d the *z*-axis, also becomes spatially dependent. The angular velocity can, if we account for the possibility that there is more than single quantum coherence ($n = 1$, i.e. when the states of the spin system differing in spin quantum number by one unit), thus be written as

$$\omega_{eff}(n, \bar{r}) = n(\omega_0 + \gamma(\bar{g} \cdot \bar{r})) \qquad \textbf{eq. 5}$$

where γ is the gyromagnetic ratio and $\bar{g}$ is as the time varying gradients.

In the presence of a magnetic field gradient, the cumulative phase shift for a single static spin is given by

$$\phi(t) = \gamma B_0 t + \gamma \int_0^t g(t') \cdot x(t') dt' \qquad \textbf{eq. 6}$$

where the first term represents the phase accrual due to the static B_0-field and the second term represents the effects of the magnetic field gradient, t, the duration of the gradient, and x the spatial location of the spin along the direction of the applied gradient[6]. The above described relationship provides the means to use a magnetic field gradient to label the spin to an initial position, with respect to the direction of the gradient, by means of small differences in the Larmor frequency.

One of the first and most basic pulse sequences used to detect spin displacements were a pulsed gradient spin echo (PGSE) designed by Stejskal and Tanner in 1965[7]. This pulse sequence consists of a 90˚ pulse followed by two gradient pulses positioned around an 180˚ pulse (see **Figure 1**).

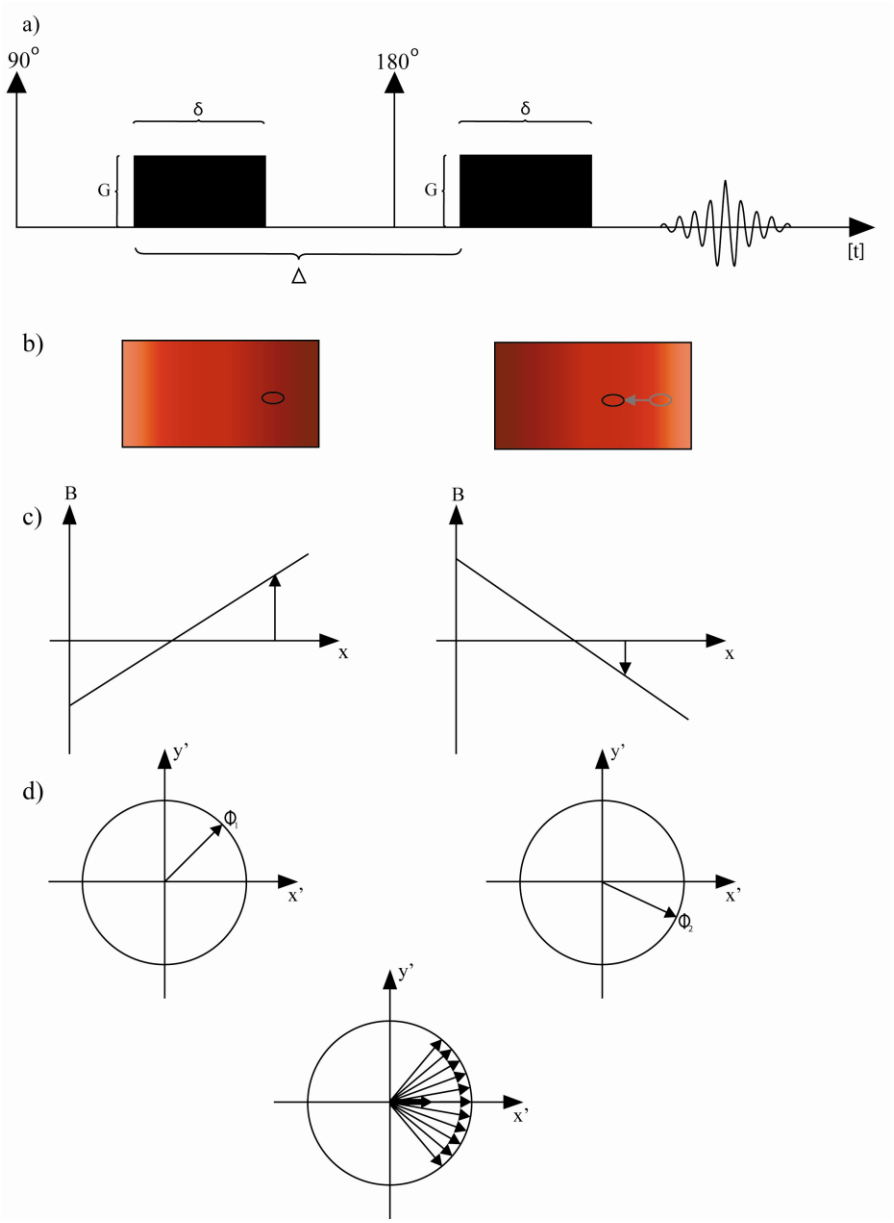

Figure 1. (a)The PGSE sequnce applied on a moving spin (b). The second gradient block has the opposite effect on the phase of the spins as the first (c) because of the 180º pulse applied in between them. If a spin has moved during the encoding (d) it will cause a net phase not equal to zero. If no movement occurred during the encoding the net phase equals to zero (d) (at the very end).

The direction of the applied gradient decides in which direction the diffusion is being measured. If for example the diffusion gradient is applied along the x-axis it causes different changes in phase depending on where the spins are located on the x-axis. When the 180˚ pulse is applied the phase of the spins are inverted. Thus, when the following gradient pulse is applied it has the opposite effect on the phase as the first gradient. In the absence of motion or diffusion the dephasing before the 180˚ pulse is exactly reversed after the second pulse because the spins experience the same magnetic field throughout. If instead the spins have experienced a drift, such as diffusive motion, between the two diffusion gradients there will only be a partial refocusing of the spins and therefore the signal amplitude will be reduced. The amount of diffusion attenuation of the signal depends on two factors; the diffusion properties of the sample determining the motion of the spins, and secondly, the pulse

sequence parameters determining the duration and amplitude of diffusion gradients and the time during which the diffusive motion takes place.

Diffusion imaging

When determining the total diffusion encoding effect of a pulse sequence a correct estimation of the diffusion sensitivity can be determined by solving

$$b = \gamma^2 \int_0^{TE} \left\{ \int_0^{\tau} G \, dt \right\}^2 d\tau \qquad \textbf{eq. 7}$$

where *G(t)* is the amplitude of all the gradient pulses in the sequence from $t = 0$ to $t = TE$. **Eq. 7** introduces the b-value, which has a major importance in diffusion-weighted imaging. The *b*-value is frequently described as the diffusion sensitisation and it is a way to relate the diffusion coefficient *D* and the signal attenuation due to the mobilization of spins during the diffusion-encoding process. This signal attenuation is described as

$$S(b) = S_0 e^{-bD} \qquad \textbf{eq. 8}$$

where *S(b)* is the signal attenuation as a function of the b-value and S_0 is the signal without diffusion encoding. The *b*-value is frequently given in s/mm^2. The above equation was an extended version (made by Le Bihan[8]) of the so called Stejskal-Tanner Equation which was introduced as together with the PGSE sequence by Stejskal and Tanner. The Stejskal-Tanner Equation[8], which is a simplification of **eq. 7**, is written as

$$b = \gamma^2 G^2 \delta^2 T_D = \gamma^2 G^2 \delta^2 \left(\Delta - \frac{\delta}{3} \right) \qquad \textbf{eq. 9}$$

where δ is the duration of the pulse, T_D is the effective diffusion time and Δ is the pulse separation. Note that the Stejskal-Tanner equation is only valid when diffusion gradients are approximated as two rectangular shaped gradients[5].

The diffusion coefficient, *D*, can be calculated with a minimum of two measurements, with and without diffusion weighting. To obtain a more accurate diffusion coefficient, a more time consuming calculation with more than two *b*-values should be used.

In biological matter the diffusion coefficient is influenced by such things as the tissue geometry, cellular viscosity and permeability[11]. Therefore, in MRI the diffusion coefficient is often designated as the ADC[9]. Other things that might influence the ADC value is capillary blood flow (perfusion) which can be seen as a fast diffusing component in grey brain matter.

For *in* vivo measurements the ADC is commonly divided into two parts; ADC_{fast} and ADC_{slow} (see **Figure 2**). There is big disagreement today of what these two parts really represent. One idea is that they represent the intra and extra cellular water.

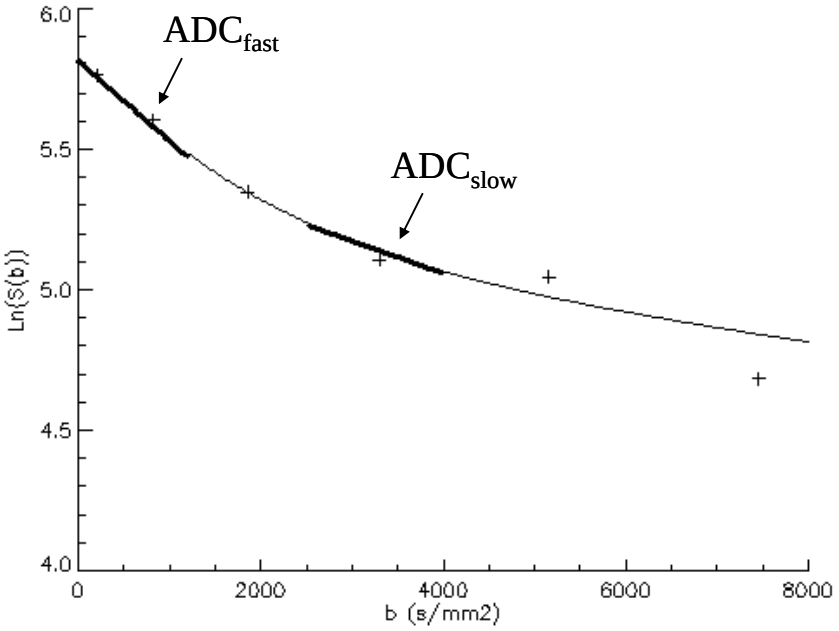

Figure 2. The ADC is determined as the slope of the signal attenuation curve. It can be divided into two parts, ADC_{fast} and ADC_{slow}. This is a simulated signal attenuation curve for diffusion in the white matter of the human brain.

When imaging gradients are introduced into the diffusion sequence they might influence the diffusion weighting. This can lead up to greater or smaller echo attenuation than expected and if not corrected for it results in an erroneous estimation of the *D*-values. The interaction between imaging and diffusion gradients is generally referred to as cross-term interaction. These cross-term interactions can be derived from the solution of **eq. 7**.

Diffusion tensor imaging

Diffusion can either be isotropic, when it's supposed to be equal in all directions, or anisotropic, when it's different for different directions. In a cylindrical structure, such as a fibre, the diffusion is anisotropic since a water molecule moves freely along it while the diffusion is restricted across it. In such a media where the measured diffusivity is known to depend upon the orientation of the tissue or the fiber bundles, no single scalar ADC can characterize the water mobility. The so called diffusion tensor can instead be used as an analytical tool in such cases and this method is generally called diffusion tensor imaging (DTI). For anisotropic diffusion, seen in for example cerebral white matter, the diffusion coefficient is described by a three dimensional tensor, i.e.

$$\bar{D} = \begin{pmatrix} D_{xx} & D_{xy} & D_{xz} \\ D_{yx} & D_{yy} & D_{yz} \\ D_{zx} & D_{zy} & D_{zz} \end{pmatrix} \qquad \textbf{eq. 10}$$

For free water molecules $D_{ij} = D_{ji}$ and the diffusion tensor reduces into a six coefficient tensor.

For DTI, one image for $b = 0$ s/mm^2 and DW images from at least six different directions are required. The more directions included for the tensor analysis, the more accurate the observed result will be.

By diagonalizing $\bar{D}$ (**eq. 10**) the eigenvalues λ_1, λ_2, and λ_3 can be determined, i.e.

$$\bar{D} = \begin{pmatrix} \lambda_1 & 0 & 0 \\ 0 & \lambda_2 & 0 \\ 0 & 0 & \lambda_3 \end{pmatrix} \begin{pmatrix} \varepsilon_1 \\ \varepsilon_2 \\ \varepsilon_3 \end{pmatrix} \qquad \textbf{eq. 11}$$

where ε_1, ε_2 and ε_3 are the eigenvectors of $\bar{D}$. For isotropic diffusion the eigenvalues are equal and after multiplication with the eigenvectors they describe a sphere. When looking at anisotropic diffusion this sphere becomes more like an ellipsoid pointing out the foremost direction of diffusion.

The larger the ratio between the eigenvalues is, the more anisotropic the diffusion in the studied media is. This ratio between the eigenvalues is often described by the fractional anisotropy (FA) index, which is determined as

$$\mathrm{FA} = \frac{\sqrt{(\lambda_1 - \langle \bar{D} \rangle)^2 + (\lambda_2 - \langle \bar{D} \rangle)^2 + (\lambda_3 - \langle \bar{D} \rangle)^2}}{\sqrt{\lambda_1^2 + \lambda_2^2 + \lambda_3^2}} \qquad \textbf{eq. 12}$$

Non Gaussian diffusion

Several years ago, in the mid 1990s, non-Gaussian diffusion was observed in neuronal tissues when using DWI. This revealed a pool of water molecules with highly anisotropic and restricted diffusion[10]. For restricted diffusion the diffusing particles are assumed to be confined to a reflecting sphere of radius *R* (the spin is neither transported through nor relaxed by the boundary). By **eq. 13**, a dimensionless variable, ξ, is defined for characterizing the restriction as

$$\xi = \frac{D\Delta}{R^2} \qquad \textbf{eq. 13}$$

For diffusing particles confined to a reflecting boundary the importance of Δ is highly significant. For short Δ the particles have not moved far enough to feel the effect of the boundaries, i.e. $\xi << 1$. This means that the measured diffusion coefficient will be the same as for freely diffusing particles. For finite Δ, i.e. $\xi \approx 1$, some particles will feel the restriction and the mean squared displacement along the measuring direction will not follow Δ linearly. For very long Δ the particles can only travel a certain distance limited by the boundaries and the diffusion coefficient becomes independent of Δ, thus making the signal attenuation sensitive to size and shape of the constrained geometry[7]. Unlike free diffusion the restricted diffusion is non-Gaussian[13].

Diffusion imaging using high b-values

Callaghan did in the late 1980s show the benefits of using high b-values with NMR spectroscopy. During the 1990s several groups have done further investigations on the use of high b-values for DWI and they have showed that the water signal decay in neuronal tissue is not mono-exponential[11 12]. This implies the existence of more than one apparent diffusing component or evidence for restriction. The q-space method is in such cases a beneficial tool for analysing the obtained data.

q-space imaging

In DWI the observed spins are being labeled to an initial position and then decoded for their motion at two separate time points. The observed echo decay depends on the diffusion time

(T_D) and the molecular displacement, as stated previously in **eq. 8**. However, **eq. 8** is not ideal for analyzing multi-exponential signal decays, as seen for example in white matter (WM) at high *b*-values[13]. Instead, the *q*-space imaging method might prove to be a very useful tool in such cases.

For a rectangular gradient pulse a phase shift is introduced as seen in **Figure 1**. During the diffusion time T_D the proton has moved to the position $\bar{r}_1$ and thus causing a net phase shift of

$$\phi = \gamma\delta\bar{G}\cdot\ \bar{r}_1 - \bar{r}_0 \qquad \textbf{eq. 14}$$

where ϕ is the phase shift and $\bar{r}_0$ represents the position of the water proton at the instant of the pulse. Every phase term $e^{i\gamma\delta\bar{G}\cdot\ \bar{r}_1-\bar{r}_0}$ is weighted by the probability for a proton to move the distance $\bar{r}_1 - \bar{r}_0$. The amplitude of the echo can thus be written as

$$S\ \bar{G}\ = \int\rho(\bar{r}_0)\int P_S\,(\bar{r}_0|\bar{r}_1, T_D)e^{i\gamma\delta G\cdot\ \bar{r}_1-\bar{r}_0}\,d\bar{r}_1 d\bar{r}_0 \qquad \textbf{eq. 15}$$

where $\rho(\bar{r}_0)$ is the spin density. By defining the *q*-vector as

$$\bar{q} = \frac{\gamma}{2\pi}\delta\bar{G} \qquad \textbf{eq. 16}$$

the amplitude of the signal is described by

$$S\ \bar{G}\ = \int\rho(\bar{r}_0)\int P_S\,(\bar{r}_0|\bar{r}_1, \Delta)e^{i2\pi\bar{q}\cdot(\bar{r}_1-\bar{r}_0)}d\bar{r}_1 d\bar{r}_0 \qquad \textbf{eq. 17}$$

When the inverse Fourier transform is applied to **eq. 17** a displacement probability distribution is obtained. This propagator, $P(\bar{r}_0, \bar{r}_1, \Delta)$, gives the probability of a spin travelling the distance $\bar{r}_1 - \bar{r}_0$ during the time Δ (**Figure 3**).

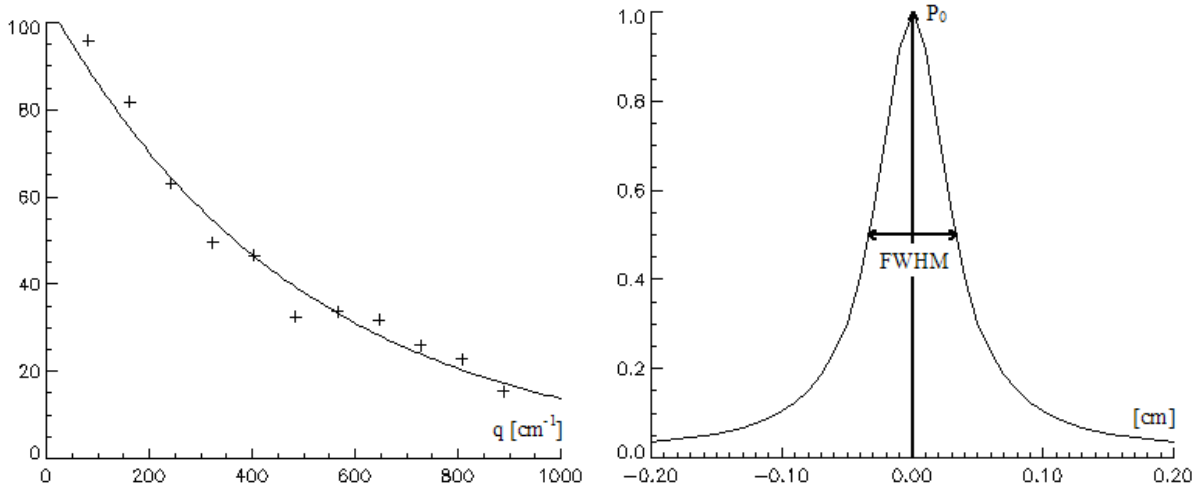

Figure 3. When the signal attenuation curve as a function of q (left) is Fourier transformed one obtains a probability density distribution of the diffusion. From this distribution it is possible to extract information regarding the FWHM (right) and the probability for zero displacement. *P(d)* is the probability for a particle to move a certain distance.

The full width at half maximum (FWHM)

FWHM is determined from the probability density function retuned by the Fourier transform of the signal versus q-attenuation curve.

The FWHM can be used for characterizing the propagator and relation to the mean square dynamic displacement is given as

$$\mathrm{FWHM} = 2\sqrt{4DT_D \ln 2} \qquad \textbf{eq. 18}$$

The root mean square (rms) displacement, closely related to the FWHM described in **eq. 18**, is defined as

$$\bar{r}_1 - \bar{r}_0 \;_{rms} = \sqrt{2n_d DT_D} \qquad \textbf{eq. 19}$$

eq. 18 together with **eq. 19** can thus give the diffusion coefficient, since

$$\bar{r}_1 - \bar{r}_0 \;_{rms} = \sqrt{2n_d DT_D} = 0.425\mathrm{FWHM} \qquad \textbf{eq. 20}$$

For molecules confined to certain spherical or cylindrical geometry, the displacement probability distribution function relates to the size and shape of the compartment if a long Δ is chosen. The *q*-space analysis was developed assuming the short gradient pulse (SGP) approximation which states that $\delta << \Delta D/a^2$ (where *a* is the confinement size) and $\delta << \Delta$, i.e. the duration of the diffusion gradient pulses must be short enough to avoid motion while they are on. As stated in **eq. 13** Δ must be chosen with consideration to the mean diffusivity and the cell size of the studied sample.

The SGP approximation is achievable for NMR spectrometers where the gradient strengths are in the order of 10 T/m, whereas in a clinical MRI environment the gradients are normally not strong enough to achieve high *q*-values.

The resolution of the *q*-space measurements is given by $1/2q_{\max}$[14]. A high *q*-value is needed since the resolution has to be smaller than the measured FWHM. A resolution of about two times the studied size is thus needed for a correct determination.

A correction to the *q*-values to account for the cross-term interaction allows a more accurate *q*-space analysis. Since the cross-term effects in the phase direction cancel out, only corrections to the *q*-values in the read and slice direction is needed[15].

Although clinical MRI scanners cannot produce gradient pulses strong enough to obtain the SGP approximation, studies have proved the success in using the FWHM as a diagnostic tool[16]. The probability of zero displacement, *P(0)*, has also been found to be beneficial. The violation of the SGP approximation in clinical MRI results in an underestimation of the confining geometry obtained from the FWHM[17]. The FWHM will in contrast be overestimated for small *q*-values due to the resolution limit 1/*q*.

Imaging sequence- STEAM

In clinical DW-MRI a SE-based sequence is often used. However, for the purpose of q-space imaging where we especially want to study effects of diffusion times the stimulated echo acquisition mode is more favorable.

The STEAM pulse sequence (Stimulated Echo Acquisition Mode), which can be used for diffusion measurements and is especially advantageous since it allows for long diffusion times. It utilizes three 90˚ RF pulses. With the first pulse the spins are flipped to the xy-plane where they are labeled by a diffusion-encoding gradient. A second 90˚ RF pulse then flips the spins back into the *z*-direction where only *T1*-relaxation is present. During this time the spins are thus unaffected by *T2**-relaxation. After a time, called the mixing time (*TM*), the third 90˚

RF pulse is applied and the spins are once again flipped into the xy-plane where the signal is detected using an EPI readout mode, after the application of another diffusion-encoding gradient.

The two gradients, in **Figure 4**, switched on during *TM* are used to cancel eddy currents and spoil signal produced by the second 90˚ RF pulse.

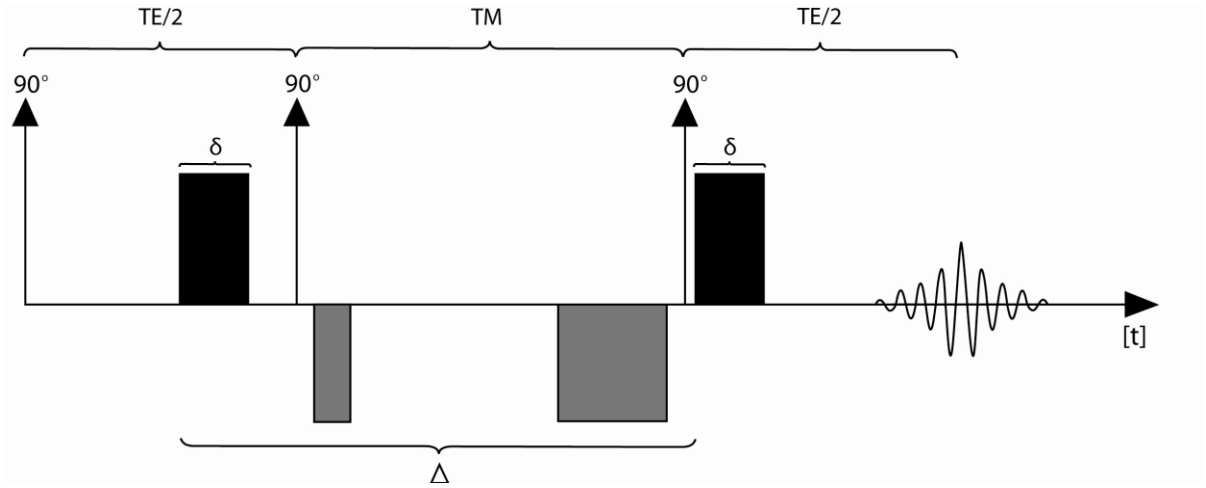

Figure 4. The STEAM pulse sequence utilizes three 90˚ RF pulses. The two black blocks symbolize the diffusion encoding gradients, and the gray blocks symbolize the gradients used for Eddy current compensation and spoiling of unwanted signal contributions. The total width of the black blocks should equal to the total width of the gray blocks.

Eddy currents occur because of the rapid switching of strong gradients in DWI which results in a rapidly changing magnetic flux inside the MRI scanner. A time varying magnetic flux through an area, *Ω*, induces an electromotive force, *emf*, given by Faraday's law of induction, i.e.

$$emf = -\frac{\partial \Phi}{\partial t} = \int_{\Omega} \frac{\partial B}{\partial t} \cdot dA \qquad \textbf{eq. 21}$$

It is these induced currents that are commonly referred to as eddy currents (EC). The EC can originate in any conductive part of the scanner and it scales with the increasing strength of the gradient pulses. The main problem with these induced currents is that they set up magnetic field gradients persisting after the primary gradients.

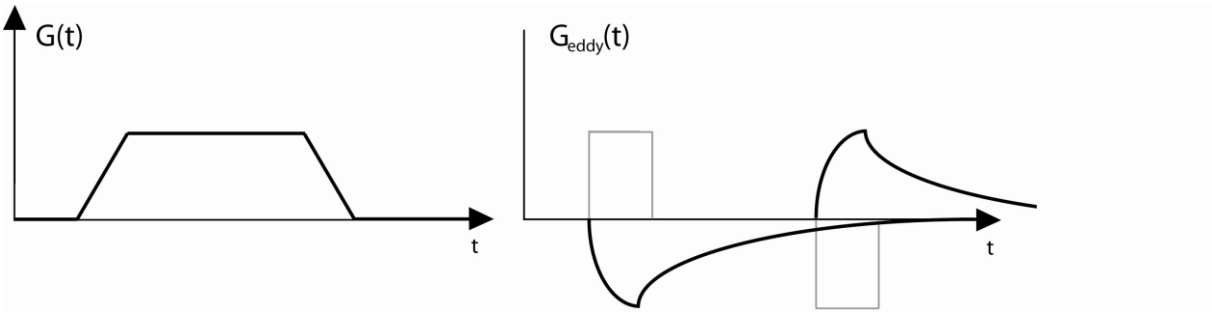

Figure 5. The slopes of the gradient G(t) induces EC $G_{eddy}(t)$ seen as solid lines. The inducing dG/dt is seen as grey lines (right).

These gradient errors produce geometric distortion in the final images. The distortions are visible as contraction or dilation of the images, or an overall shift and shear[17].

The best cure for EC is to use self-shielded gradient coils which has additional wiring to decrease the effects of gradients outside the gradient coils. Another way to decrease the effects of EC is to purposely altering the shape of the currents sent to the gradient hardware.

However, they can also be partly compensated for by intelligent sequence design (e.i. in the STEAM sequence), or by post-processing of the images.

Materials and method

Prestudy - Choice of phantom

The prestudy was done both to find a suitable phantom for the study of anisotropy and to find out how the further experiments should be organized.

The first step in the process of finding a suitable phantom for diffusion in an anisotropic media was to consult the literature. Several suitable phantoms were identified such as celery[18] and asparagus[3].

The first phantom evaluation made on the scanner was performed on an arrangement of carrots and rhubarbs, which are both vegetables with a structure resembling the ones found in literature. The second phantom consisted of leek, rhubarb, banana and asparagus. All of these vegetables should intuitionally have a structure with high anisotropy.

Evaluation of the different phantoms was performed using a Siemens Allegra 3T head scanner equipped with 40 mT/m gradients. The different phantoms, which consisted of different vegetables, were submerged in a water-filled plastic box and aligned parallel to the main magnetic field. The signal was sampled for 16 equidistant q-values and six diffusion encoding directions were used. In-house developed stimulated echo pulse sequence (STEAM) was used to evaluate diffusion measurements with four different T_D:s. A TR of 3000 ms and a voxel size of 1.3×1.3×10 mm^3 was used in the experiment. Other sequence acquisition parameters used in the experiment were as showed in **Table 1**.

Table 1. Imaging parameters for the four different diffusion times used in the experiment.

T_D [ms]	TE [ms]	q [cm^{-1}]	δ [ms]
24	125	10-126	6
87	200	10-280	15
150	267	10-350	18
200	317	10-350	18

Since the asparagus proved to have the highest anisotropy and an overall high signal in the DW images, the further experiments were carried out on this vegetable. A set of images with the asparagus aligned in the x, y and z – directions was obtained in order to validate the directional dependence of the fibers. Signal curves, ADC, FWHM, and FA maps were calculated using a locally developed IDL program designed for analysis of the DW images.

Mean signal in ROI:s placed in the DW images of the vegetables were calculated and plotted as a function of the *q*-values. This plot could then be used for investigation of the restriction of the studied boundary.

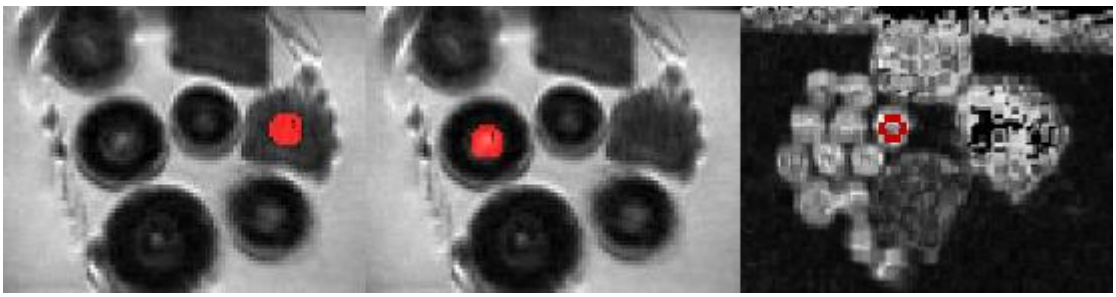

Figure 6. The employed ROI:s in the rhubarb (left) and in the carrot (middle) and in the DW image of the asparagus (right).

q-space measurements

In order to assess the anisotropy and any existing degree of restriction in asparagus, two different protocols were evaluated one for measurements in three orthogonal directions and one for conventional DTI evaluation. The measurements in the orthogonal directions were performed using six directions (x, -x, z, -z, y and -y), which means that this method includes measurements directly along the fibers as well as perpendicular to them. The DTI protocol was also based on measurements carried out in six directions but in this case a tensor analysis was performed since no measurements are carried out directly along the fibers.

The parameters were set as equal as possible for the two different measurements to facilitate the comparison between them. Common imaging parameters were as follows: FOV = 87 mm^2, slice thickness = 10 mm, imaging matrix = 128×128 (yielding a voxel size of $0.7\times0.7\times10$ mm^3).

Orthogonal directions (XYZ)

The asparagus was positioned in the same plastic box that was used in the pre-study. A repetition time of 4500 ms was used and the NEX was set to 4. Using a constant echo time (*TE*) of 89 ms and varying mixing times (*TM*) of 101, 141, 181, 220 and 258 ms, different diffusion times (T_D) were obtained; 120, 160, 200, 240 and 280 ms. The signal was sampled for *q*-values ranging from 20-357 cm^{-1} equidistantly in 16 steps, yielding a resolution of $1/2q_{max} = 14$ μm, with $\delta = 24$ ms.

DTI-mode

A constant *TE* of 94 ms and *TM*:s of 101, 141, 181, 220 and 258 ms led to T_D:s of 120, 160, 200, 240 and 280 ms. A varying repetition time of 2500-3500 ms was used and the NEX was set to 3. The signal was sampled for *q*-values ranging from 20-357 cm^{-1} equidistantly in 16 steps, yielding a q-resolution of $1/2q_{max} = 14$ μm, with $\delta = 24$ ms.

Data post processing

No zero filling were made on the *q*-space signal data. Filtering in the wavelet domain (for description see Appendix A) was used to denoise the complex images and increase the overall signal to noise ratio. Regions of interest (ROI) were positioned in the parametric maps according to **Figure 7**. Note that the centre of the asparagus was not included in the ROI since it gave only a very low signal. A ROI was also selected in the surrounding water.

Figure 7. The used ROI, placed in the FWHM map.

Parametric maps of the FWHM of the diffusion propagator were calculated. In both the XYZ and the DTI measurement the FWHM has been plotted as a function of $\sqrt{T_D}$. The only difference is that a tensor analysis of the FWHM has been done for the DTI measurement which gives us results given as eigenvalues, $\boldsymbol{\lambda}_1$, $\boldsymbol{\lambda}_2$, $\boldsymbol{\lambda}_3$, where $\boldsymbol{\lambda}_1$ represents the free direction and $\boldsymbol{\lambda}_3$ represents the restricted direction in the asparagus. This is not a conventional procedure but it has been proved to be an accepted method[19], and it is done to compensate for the fact that no measuring direction in the free direction has been included in the DTI experiment.

Microscopy

As validation for the determination of the structural sizes in the asparagus, microscopy images were obtained using a Zeiss WL research microscope (see **Figure 8**).

The asparagus was cut into thin slices, both in the perpendicular and parallel to the fiber direction. The slices were cut from the asparagus at different positions (4 cm, 12 cm and 20 cm from the top). Theses slices were then photographed through the microscope. The photos were analysed by measuring the sizes of the visible structures and then compared with the results from MRI scanner. The sizes were calculated as a mean of capillary sizes within a couple of bundles.

Figure 8. The used Zeiss WL research microscope.

Results

Prestudy - Choice of phantom

The signal curves for six different directions obtained from the first measurement on carrots and rhubarbs are shown in **Figure 9** and **Figure 10**, plotted as a function of q. The signal

curves from the rhubarb reveal a little more anisotropy, seen as a divergence of the signal decay curves, than the signal curves determined from the DW images of the carrot.

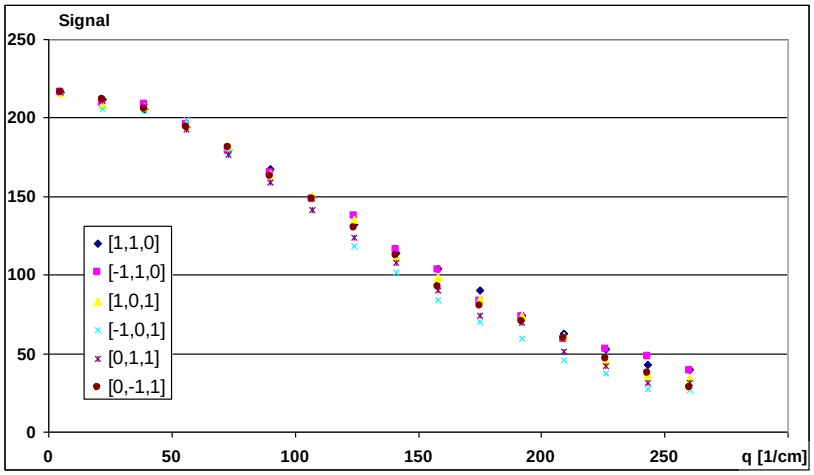

Figure 9. Signal curves from the rhubarb in six different directions.

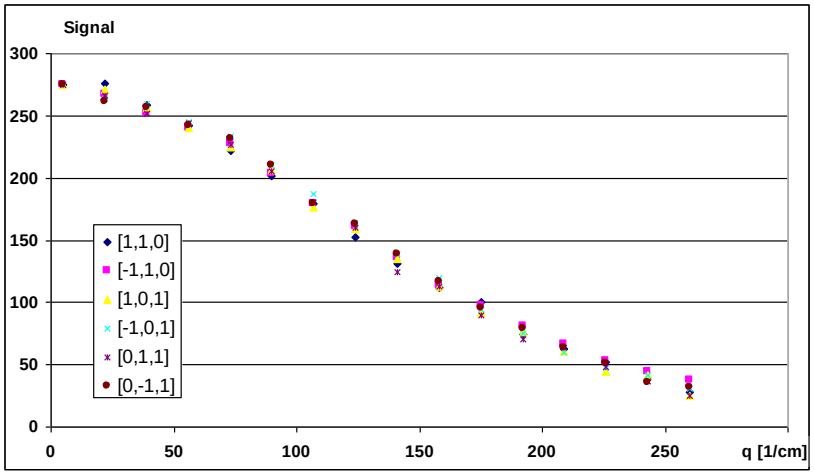

Figure 10. Signal curves from the carrot in six different directions.

The signal curves obtained from the asparagus in the second phantom are shown in **Figure 11**. There is clear difference between the signal curves in the trans-fiber direction compared as to what is seen in along[1] the fibers.

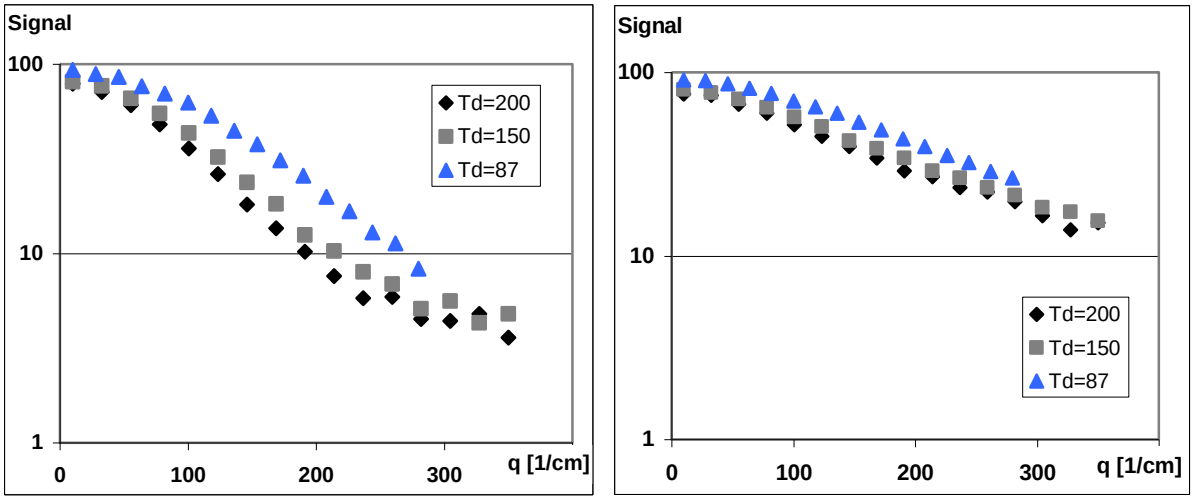

Figure 11. Left: Signal decay as a function of q for three different T_D (200, 150 and 87 ms) in the least hindered direction of the asparagus, along the fibres. Right: Same as the left but for the most restricted direction, perpendicular to the fibres.

In **Figure 12** the ADC and the FWHM as a function of T_D for the different diffusion directions is plotted. There is a small decrease in the ADC as a function of T_D both in the restricted and in the "free" directions (except for direction [0,1,1]). The FWHM for the corresponding diffusion directions do not differ much for the shortest T_D. As the T_D increases the difference becomes more prominent with increasing FWHM in the assumed free directions whereas it stays constant (or it is a very, very small decrease) in the more restricted directions.

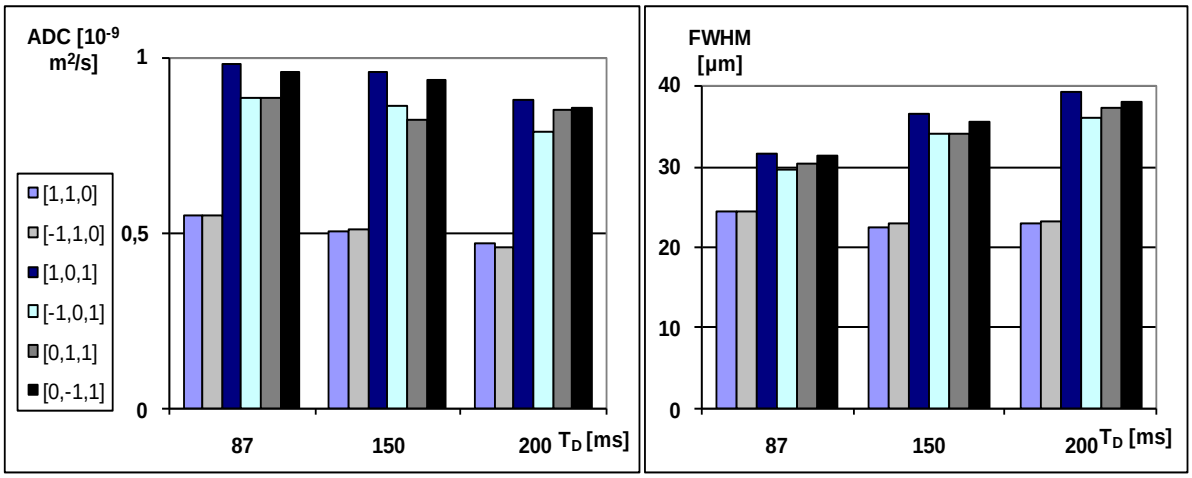

Figure 12. ADC in asparagus for three different T_D (87, 150 and 200 ms) for the applied six diffusion directions.

[1] One should keep in mind that no measurements have been performed in the exact free direction of the asparagus, along the fibres.

Regarding the FA obtained from the FWHM[17] (i.e. FA (FWHM)) we see that they show a legible anisotropy. It is seen in **Figure 13.** In this figure we also see FA obtained from the ADC value (i.e. FA (ADC)).

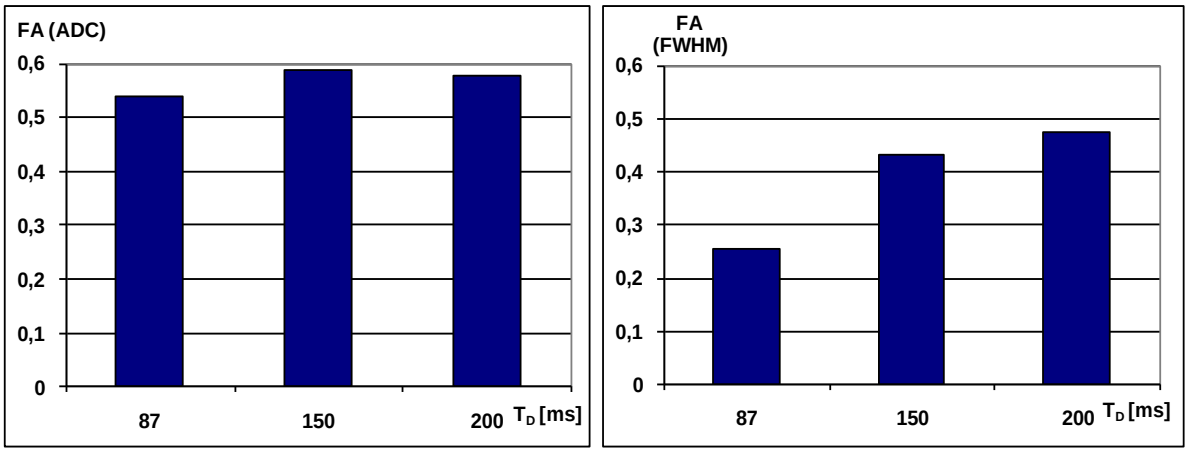

Figure 13. FA (ADC) and FA (FWHM) in asparagus for three different T_D (200, 150 and 87 ms).

In **Figure 14** below, the FWHM perpendicular and parallel to the fibres is plotted as a function of the $\sqrt{T_D}$ for the two different measurements performed on asparagus as described above.

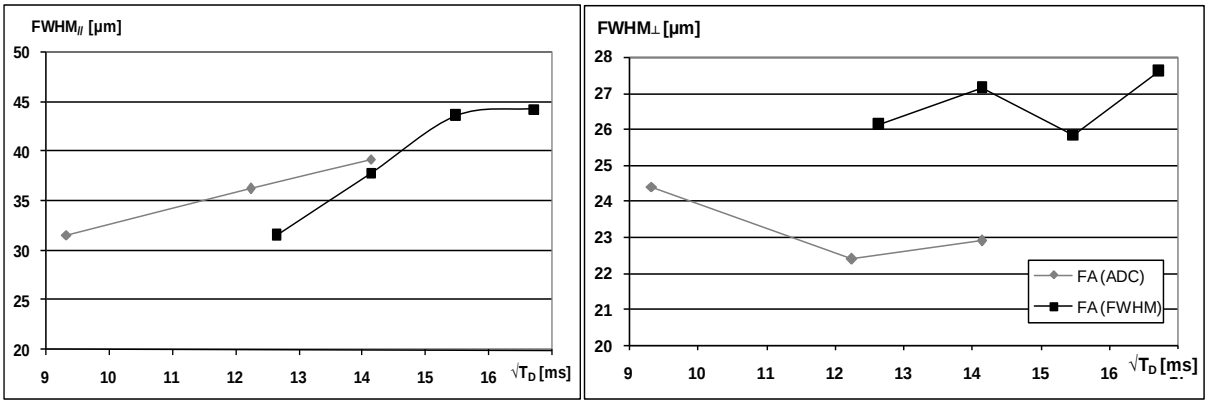

Figure 14. FWHM as a function of $\sqrt{T_D}$ along the fibres (left) and perpendicular to the fibres (right) in the asparagus.

In **Figure 15.** we see different FA maps explained in the caption.

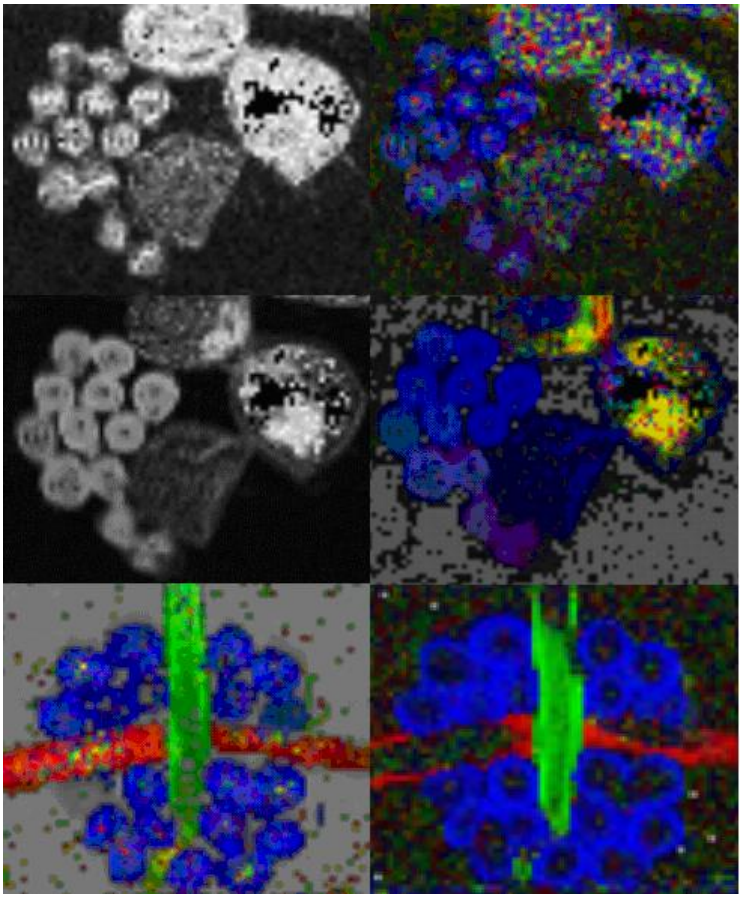

Figure 15. Upper row: conventional FA $_{ADC}$ and colour coded largest eigenvalue direction, second row: conventional and colour coded FA $_{FWHM}$, third row: color coded larest eigenvalue directions FA_{ADC} and FA_{FWHM}. The red color represents the left-right diffusion direction, the green color represents the up-down direction and the blue is for the in-out direction. The FA maps are made on the asparagus positioned in the x, y and z – direction. T_D is here chosen to be 150 ms.

q-space measurements

Orthogonal directions (XYZ)

The result obtained from the measurement performed in the orthogonal directions is shown in **Figure 16** and **Table 2**. In the free directions of the asparagus, along the fibers, and in the water, the FWHM increases for increasing T_D. In the restricted direction, perpendicular to the fibers the FWHM stays constant as the T_D increases. The mean FWHM calculated from the restricted directions (x- and y directions) is 31µm. The FWHM in the free direction (z-direction) is linearly increasing as a function of T_D, similarly as seen for the freely diffusing water.

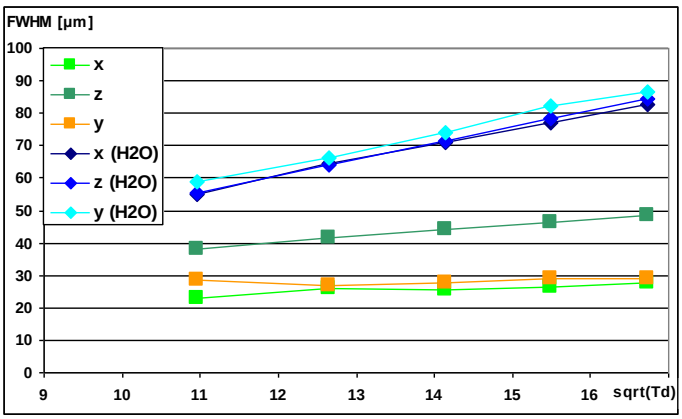

Figure 16. FWHM as a function of $\sqrt{T_D}$ for asparagus and water.

Table 2. Resulting FWHM-values from the orthogonal measurements.

T_D[ms]	$FWHM_{asparagus}$		$FWHM_{H2O}$
	mean(xy) [µm]	Z [µm]	Z[µm]
120	29.0	41.6	55.3
160	30.4	46.1	64.1
200	31.5	49.4	71.4
240	32.6	52.0	78.2
280	33.3	54.0	84.6

DTI-mode

The result obtained from the measurement performed in the conventional DTI mode is shown in **Figure 17** and **Table 3**. In the free directions of the asparagus, along the fibers, and in the water the FWHM increases for increasing T_D. In the restricted direction, perpendicular to the fibers the FWHM is constant as the T_D increases. The mean FWHM calculated from the restricted direction (λ_3) is 24µm. The FWHM in the free direction (λ_1) is linearly increasing as a function of T_D, similarly as seen for the freely diffusing water.

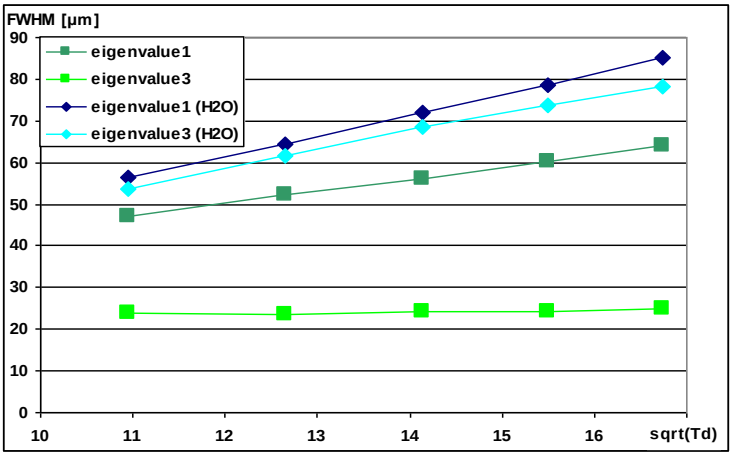

Figure 17. Eigenvalues as a function of $\sqrt{T_D}$ for asparagus and water. Eigenvalue 1 represents the parallel direction while eigenvalue 3 represents the perpendicular direction.

Table 3. Resulting eigenvalues from the DTI-measurement.

T_D [ms]	λ_1 [µm]	λ_3 [µm]	λ_1 (H_2O) [µm]	λ_3 (H_2O) [µm]
120	47.2	23.8	56.5	53.5
160	52.2	23.4	64.3	61.5
200	56.2	24.3	72.0	68.5
240	60.4	24.4	78.5	73.8
280	64.0	24.8	85.1	78.4

Microscopy

The analyzed microscopy images reveal structures, as seen in **Figure 18.** Bundles of vascular structures are seen among the parenchyma cells, which make up the bulk of the plant structure.

Each capillary seen within the black circle in **Figure 18** has a diameter of 24.9 ± 6.1 µm.

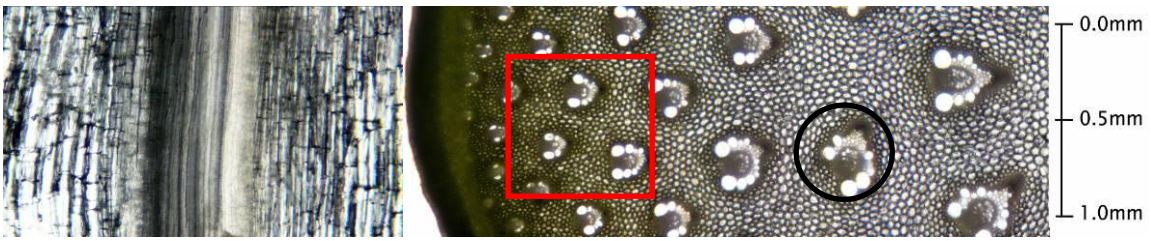

Figure 18. To the left a microscopy image of the asparagus along the fibres, and to the right an image across the fibre structure. The white structures within the black circle above has a diameter of 24.9 ± 6.1 µm. The red square represents the size of the voxel chosen in the XYZ/DTI measurements.

Discussion

The choice to use asparagus as a phantom in this study was based on "trial and error", in other words by trying some different plants, which have a well-known fibrous morphology.

However, this is not the first study in which the asparagus is successfully used as a phantom for anisotropic diffusion. Boujraf *et al*. used asparagus to study the value of acquisition and post processing techniques commonly used in the clinic for anisotropic diffusion experiments[20]. They concluded that the known structural information about the main cell types correlates well with the behaviour of the diffusion parameters. They did however not perform q-space analysis in such a way that I've done.

Sigmund and Song also used asparagus in their multiple echo diffusion acquisition technique experiments[21]. They confirmed the anisotropy present in the asparagus and thus the advantage of using this plant for such studies.

The initial part of the study was aimed for selecting a proper phantom but the early measurements were also used to better understand how the further experiments should be carried out.

The greater difference seen between the signal decay curves for the different diffusion encoding directions, the more anisotropic behavior of the diffusion is present in the studied media. The signal curves in **Figure 9** and **Figure 10** reveal only a slight anisotropy in the rhubarb, and even less in the carrots, i.e. the signal diverges more between the different directions in the rhubarb than in the carrot. Further optimizations, such as changing the diffusion parameters, have to be performed if these vegetables should work as phantoms for anisotropic diffusion. Since neither the carrots nor the rhubarbs showed the desired properties, other vegetables such as leek, banana and asparagus were tried out. The second set revealed a high anisotropy in the asparagus, which motivated further analysis of it.

The asparagus is a vegetable, or to be more precise the shoots of *Asparagus officinalis*. The green plant consists of parenchyma and vascular bundles. The parenchyma cells are thin-walled cells of the ground tissue, making up the bulk of the plant structure[22]. The vascular bundle is a component in the transport system of a vascular plant. The vascular tissue consists of xylem and phloem. The xylem is generally positioned adaxial (closer to the center of the stem or root), while the phloem is positioned abaxial (closer to the exterior of the plant)[23]. The central part of the stem contains thick walled cells, which provide strength and support to mature plant structures, and they may be dead at functional maturity. The sizes of the highly organized but asymmetric structures in the asparagus make it suitable as a phantom in DWI. The different T_D:s have a decisive influence on our possibility to conclude whether we see a restriction or not in the vegetable structure. The signal attenuation curves from the asparagus, seen in **Figure 11**, become steeper as the T_D is increased. As the T_D increases the

displacement of the water molecules enlarges and thus results in a larger amount of signal loss. The diversity of the curves is greater for the different T_D:s in the "free" direction than across the fibers and thus revealing a behavior of an anisotropic structure.

The difference between the ADC in **Figure 12** for the different directions comes from the difference in restriction. High restriction results in a low ADC. But the differences can also be a result of cross-term effects. The result shows a small decrease of ADC as the T_D increases in both the restricted and the "free" direction. Since the noise influence the ADC it might be a disturbing factor in this result. The FWHM as a function of the T_D, also seen in **Figure 12**, increases in the "free" direction, while it stays constant for the restricted direction. The result corresponds well to an anisotropic behavior in a fiber with a diameter of about 23 µm.

The FA which in **Figure 13** emphasizes what the other results is indicating, i.e. free diffusion along the fibers and restricted across them. The reason why the two different FA results in Figure 13 differ so much is probably because of their origin. The FA_{ADC} represents a fast diffusion component while the FA_{FWHM} represents both a fast and a slow component.

For free diffusion FWHM should increase linearly with increasing $\sqrt{T_D}$ and for restricted diffusion the FWHM should not change as T_D increases. In **Figure 14** an increase in FWHM can be seen although it's not exact linear. For restricted diffusion the FWHM should not change as T_D increases, which is also seen in this figure.

One should keep in mind that no measurements have so far been performed in the exact free direction of the asparagus, along the fibres.

Orthogonal directions (XYZ)

From the results shown in **Figure 16** one sees the water as freely diffusing with a linear increase of the FWHM as a function of $\sqrt{T_D}$.

In the free direction of the asparagus, the FWHM of the water also seems to increase linearly as a function of $\sqrt{T_D}$, while it is constant for the two directions across the fibers (x- an y-direction). A mean FWHM taken from the two directions across the capillaries tell us that their radius is in the order of 31 µm.

The results have some bad sides even though they seem successful. The dynamic displacement profile perpendicular to the fibres of the asparagus represents the water both in the capillaries and in the surrounding cells and this might affect the result.

Another problem is that the slice thickness is 10 mm and no bending of the fibres is taken into account which implies that partial volume effects might have some effect on the result.

All the directions have been included in the measurement but it is important to position the asparagus exactly in correct direction to assure an accurate result. With the arrangement of asparagus used in this experiment I cannot guarantee that such accuracy has been pursued.

DTI-mode

Just as in the measurement in the orthogonal directions, discussed above, one sees in **Figure 17** the water as freely diffusing with a linear increase of the FWHM as a function of $\sqrt{T_D}$.

The direction along the fibers, represented by λ_1, is very closely related to the freely diffusion water with linearly increasing FWHM.

The water molecules are on the other hand restricted in the fibre-transverse direction with constant FWHM for increasing $\sqrt{T_D}$. The mean FWHM was here determined to be 24 µm, a bit smaller than what came out of the xyz-measurement.

In this experiment it was not as important as for the xyz-measurement to position the asparagus in correct direction, since a tensor analysis was done.

Microscopy

With a measured structure size of 24.9 ± 6.1 the result from the microscopy images is indicating that the results on the experiments carried out on the MR scanner are accurate.

Conclusion

Our FWHM results indicate that there exists a restriction in diffusion perpendicular to the main axis of the asparagus, with the size of approximately 24 µm. These results are in agreement with the result from the microscopy image. The FWHM parallel to the asparagus increases with $\sqrt{T_D}$, which suggest a more free diffusion in that direction. However, one should keep in mind that the dynamic displacement profile perpendicular to the asparagus represents the water both in the capillaries and in the surrounding cells and that this might influence the results.

We conclude that it is feasible to measure structural sizes in biological materials in the range of approximately 20-30 µm with a clinical MRI scanner. This is of great interest since our voxel resolution normally is in the order of millimetres.

We have showed that it's possible to measure and also quantify the restricted diffusion. The next step in the future would be to study the effects of restricted diffusion in vivo. One theory of hindered diffusion claims that in the human body the boundaries, i.e. the cell membrane, are not absolute and particles can pass through them if given enough time. Thus, this theory claims that the cell membranes are semi-permeable and for long diffusion times the otherwise hindered particles will appear as free. Another theory is claiming that the hindered diffusion appears in the extra cellular water when the molecules move around the cells[24].

Acknowledgements

I would like to give my deepest thanks to my supervisor Sara Brockstedt for always being very helpful and supporting during this semester. Her overriding knowledge in the field has come to great assistance.

I also owe enormous gratitude towards Jimmy Lätt acting as a fantastic supervisor with his enthusiasm and encouragement. There is no time he's not available online. We have had some great late night times by the scanner together!

And Marcus: you have been a wonderful colleague and friend with lots of good inputs to this work.

I would also like to thank Freddy Ståhlberg and Ronnie Wirestam for their relevant inputs and constructive criticism.

The performances with the microscopy would not have been done without the time and effort that Eric Carlemalm put into it. Many thanks to him as well!

Last but definitely not least I would like to thank Emil Nordh for his company and all the wonderful time we've had working on our thesis.

Anna Rydhög

January 25, 2007

Appendix A

Wavelet filtering

Wavelet filtering is a method used for denoising of MR-images by lowering the rectified noise floor and thereby a wider range of the signal curve can be used.

The MR raw data is stored as a complex array where the real and imaginary parts demonstrate a Gaussian noise distribution, which is required for the wavelet filtering method.

The complex signal is given by

$$x = s + n \qquad \textbf{eq. 22}$$

where *s* is the signal without noise and *n* is the Gaussian noise with a variance of σ^2. When the discrete wavelet transform is applied on the raw data the corresponding wavelet coefficients are given as

$$y = \Theta + z \qquad \textbf{eq. 23}$$

where $y = W_n x$, $\Theta = W_n s$ and $z = W_n n$ with W_n as a wavelet transform. An orthogonal wavelet converts white noise into white noise. Since the noise is uniformly spread over all wavelet coefficients the nose in the wavelet space remains unaffected.

Each wavelet coefficient is then thresholded by multiplication by the hard-threshold filter, i.e.

$$h_h(i,j) = \begin{cases} 1, if \left| y(i,j) \right| > \rho\sigma \\ 0, otherwise \end{cases} \qquad \textbf{eq. 24}$$

to obtain the filtered signal in the wavelet space, i.e. to obtain Θ of the *i*, *j*th pixel. Thus, the hard-threshold filter sets any $\left| y(i,j) \right|$ below $\rho\sigma$ and keep the remaining data unchanged. ρ is a user-defined empiric threshold factor and σ is the standard deviation of the noise. Large values of ρ result in a large degree of noise reduction, but may also lead to image smoothing and artefacts.

A Wiener-like filter is also added to further improve the images. The filter primarily affects the small wavelet coefficients and has no or little effect on the large wavelet coefficients[25].

Appendix B

Abstract ISMRM

Using q-space diffusion MRI for structural studies of biological phantom at 3T clinical scanner

A. Rydhög[1], J. Lätt[1], M. Nilsson[1], E. Nordh[1], S. Brockstedt[1], E. Carlemalm[2], R. Wirestam[1], and F. Ståhlberg[1]
[1]Medical Radiation Physics, Lund University, Lund, Sweden, [2]Department of Electron Microscopy, Lund University, Lund, Sweden

Introduction

q-space imaging is an established method in NMR spectroscopy for retrieving structural information from biological materials [1]. Structural q-space imaging at a clinical scanner is more difficult to achieve due to limited gradient performance, however apparent mean displacement data has been presented *in vivo* [2]. The aim of this study was to investigate the possibility for absolute quantification of fibre structure sizes in a biological phantom, using the Full Width at Half Maximum (FWHM) of the diffusion propagator and microscopy images were obtained as a reference.

Materials and Methods

Experiments were carried out on a Siemens Allegra 3T head scanner with 40 mT/m gradients. The phantom consisted of whole green asparagus submerged in a water-filled plastic box. The asparagus were aligned parallel to the main magnetic field. An in-house developed stimulated echo pulse sequence was used to perform diffusion measurements in the six directions x, -x, z, -z, y and -y. Other imaging parameters were as follows: FOV=95×83 mm^2, slice thickness=10 mm, imaging matrix 128×128 (yielding a voxel size of 0.7×0.7×10 mm^3), repetition time (TR) = 4500 ms and NEX=4. The complex images were denoised by filtering in the wavelet domain [3]. Using a constant echo time (TE) of 89 ms and varying mixing times (TM) of 101, 141, 181, 220 and 258 ms different diffusion times (T_D) were obtained; 120, 160, 200, 240 and 280 ms. The signal was sampled for q-values ranging from 20-357 cm^{-1} equidistantly in 16 steps, yielding a resolution of $1/2q_{max}$=14 µm [4], with δ=24 ms. No zero filling were made on the q-space signal data. Parametric maps of the FWHM of the diffusion propagator [1] were calculated. Regions of interest (ROI) were positioned in the parametric maps according to figure 1. Microscopy images were obtained using a Zeiss WL research microscope as a validation in the determination of the structural sizes

Results

The results show a linear relationship between the measured FWHM and $?T_D$ for the freely diffusing water molecules in the water outside the asparagus, as expected from theory. In the most restricted diffusion direction, across the fibre structure, the FWHM is almost constant for increased $?T_D$. The FWHM in the x- and y-direction (⊥) of the asparagus was 23.9 ± 0.8 µm. From the microscopy image, we see that the capillary system highlighted in figure 2 has a diameter of 24.9 ± 6.1 µm.

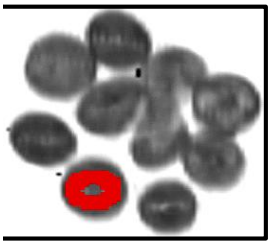

Figure 1. The used ROI, placed in the FWHM map, perpendicular to the fibres.

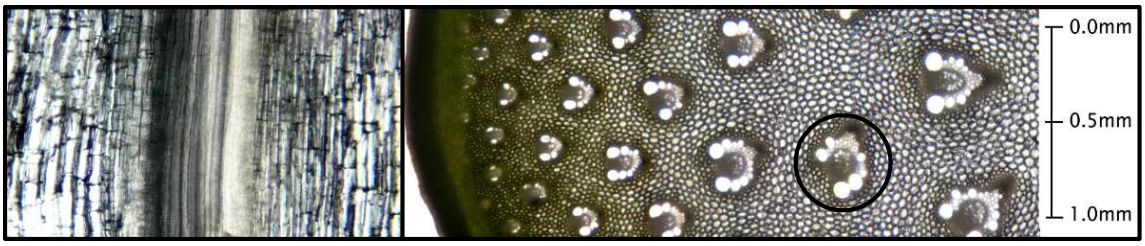

Figure 2. Left: Microscopy image of the asparagus along the fibres. Right: As left, but across the fibre structure. The bright structures within the circle above has a diameter of 24.9 ± 6.1 µm.

Discussion

Our FWHM results indicate that there exists a restriction in diffusion perpendicular to the main axis of the asparagus, with the size of approximately 24 µm. These results are in agreement with the result from the microscopy image. The FWHM parallel to the asparagus increases with $?T_D$, which suggest a more free diffusion in that direction. However, one should keep in mind that the dynamic displacement profile perpendicular to the asparagus represents the water both in the capillaries and in the surrounding cells and that this might influence the results. We conclude that it is feasible to measure structural sizes in biological materials in the range of approximately 20-30 µm with a clinical MRI scanner.

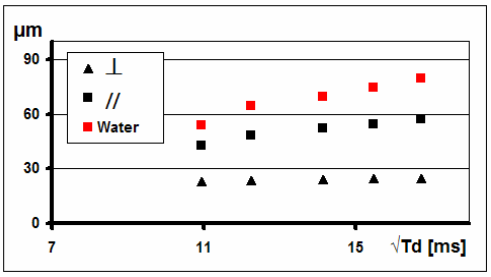

Figure 4. The diagram shows the obtained FWHM values as a function of $?T_D$.

T_D[ms]	$FWHM_{ASPARAGUS}$		$FWHM_{H2O}$
	⊥	//	
120	22.7	42.3	53.8
160	23.6	48.2	64.5
200	24.1	51.7	69.3
240	24.4	54.1	74.3
280	24.8	56.9	79.1

Table 1. The numerical results from the analysis; FWHM perpendicular (⊥), parallel (//) to the fibre structure and for freely diffusing water outside the asparagus.

References

[1] D. G. Gory, A. N. Garroway, MRM 14:435-444 (1990)
[2] Y. Assaf, *et.al.* MRM 47::115-126 (2002)
[3] R. Wirestam *et.al.* MRM 56:1114-1120 (2006)
[4] C-P Lin, NeuroImage 19:482-495 (2003)

Appendix C

Abbreviations

ADC	Apparent Diffusion Coefficient
DTI	Diffusion Tensor Imaging
DWI	Diffusion Weighted Imaging
EPI	Echo Planar Imaging sequence
FA	Fractional Anisotropy
FOV	Field Of View
FWHM	Full Width at Half Maximum
GM	Grey Matter
MRI	Magnetic Resonance Imaging
NMR	Nuclear Magnetic Resonance
RF	Radio Frequency
RMS	Root Mean Square
ROI	Region Of Interest
SNR	Signal to Noise Ratio
STEAM	Stimulated Echo Acquisition Mode
TE	Echo Time
TM	Mixing Time
TR	Repetition Time
WM	White Matter

Appendix D

Svensk populärvetenskaplig sammanfattning

Storleksbestämning på mikrometernivå med MRI

MR används som förkortning för magnetisk kärnspinn resonans, ett fysikaliskt fenomen som nyttjas inom både kemi och medicin. Inom medicin används bildgenererande MR tomografi för att studera både morfologi och funktion av en människans inre. Tekniken baserar sig på starka magnetfält och radiovågor utan användandet av kirurgi eller joniserande strålning.

En klinisk MR kamera, består oftast av en supraledande magnet med en styrka på ungefär 70 000 gånger det jordmagnetiska fältet. Då en patient ligger i en magnetkamera ställer väteatomerna i kroppen in sig som små kompassnålar börjar precessera med en hastighet som beror på magnetens styrka. Man säger att väteatomerna ställt in sig i jämviktsläge. Med hjälp av radiovågor kan man "tippa" väteatomernas rotation från den tidigare rotationsaxeln och när sedan dessa radiovågor stängs av vill atomerna återgå till sitt jämviktsläge, vilket sker under utsändandet av energi som vi kan detektera. Beroende på var väteatomerna har sitt ursprung kommer signalen att avta med olika hastigheter och man kan därför få fram bilder vars kontrast beror på skillnaden i signalavtagandet från olika organ. Man kan även göra funktionella studier där man tittar på ett organs funktion. Ett exempel är diffusionsmätningar som kvantifierar vattnets slumpmässiga termiska rörelser som är olika för olika vävnader.

Ett viktigt användningsområde av diffusions MR är tidig diagnos av blodpropp i hjärnan, något som inte kan avbildas med andra bildgivande metoder. En annan applikation av diffusions MR är då man studerar vattnets rörelse i hjärnan, vilken hindras i en riktning tvärs fibrerna i men är betydligt längre parallellt med fibrerna. På så vis kan man få fram bilder som indirekt kartlägger nervvävnadens utbredning och studerar hur den påverkas i olika sjukdomsförlopp så som demens, Parkinson, MS och olika tumörsjukdomar.

Med dagens maskiner kan man göra mätningar med betydligt högre diffusionskänslighet än vad man tidigare kunnat. Min uppgift har varit att undersöka möjligheten att överföra en teknik som används inom kemiforskningen, s.k. q-space imaging, till kliniska MR kameror. Denna teknik medför möjligheter att storleksbestämma t.ex. proteiner och cellstrukturer. Vid denna typ av studier är det viktigt att man optimerar mättiden så att man har kontroll på om vattenmolekyler anses fritt rörliga eller om de hindras i sin rörelse av omkringliggande strukturer. Om man låter mättiden vara så pass lång att vattenmolekylerna hinner studsa flera gånger mot väggarna i den undersökta strukturen, så kan storleken på strukturen bestämmas genom att man kvantifierar hur långt vattenmolekylerna rört sig. Att ta steget från vad kemisterna kan göra till att utföra det med en klinisk MR kamera är inte trivialt eftersom det är stor skillnad på utrustningens prestanda (huvudmagnetfält och gradientstyrka).

I detta arbete har ett biologiskt fantom (sparris) med strukturer i storleksordning10μm studerats. Resultaten visade tydligt att vattnet diffunderar fritt längs med fibern medan det hindras i sin diffusion tvärs fibrerna av strukturer som verkar ligga separerade med ungefär 27 μm mellanrum. Mikroskopibilder som togs, överensstämmer utomordentligt väl med dessa resultat med bilder som uppvisar strukturstorlekar på ungefär 25μm.

Detta försök, som tidigare inte utförts på en klinisk MR kamera, är ett steg mot bättre förståelse om vad man egentligen tittar på med q-space analys och förhoppningarna är att resultaten ska kunna användas för vidare studier inom ämnet. Kanske kommer vi en dag att fullt kunna förstå patologin och de bakomliggande mekanismerna för till exempel blodpropp och vad olika komponenter i hjärnan ger oss för information i diffusionsviktade MR bilder.

Bibliography

[1] M. E. Moseley, Y. Cohen, J. Mintorovitch, L. Chileuitt, H. Shimizu, J. Kucharczyk, M. F. Wendland and P. R. Weinstein. Early detection of regional cerebral ischemia in cats: comparison of diffusion- and T2-weighted MRI and spectroscopy. Magnetic Resonance in Medicine, 14(2):330-346, 1990

[2]C. Beaulieu. The basis of anisotropic water diffusion in nervous system – a technical review. NMR IN BIOMEDICINE, 15:435-455, 2002

[3] C. Delalande, J.A. De Zwart, H. Trillaud, N. Grenier and C.T.W. Moonen. An echo-shifted gradient-echo MRI method for efficient diffusion weighting. Magnetic Resonance in Medicine, 41(5):1000-1008, 1999

[4] C. A. M. Wheeler-Kingshott, G. J. Barker, S. C. A. Steens, M. A. van Buchem. *D*: the Diffusion of Water. *Quantitative MRI of the Brain: Measuring Caused by Disease*. John Wiley & Sons, 2003

[5] WS. Price. Pulsed-Field Gradient Nuclear Magnetic Resonance as a Tool for Studying Translational Diffusion: Part 1. Basic Theory. Concepts of Magnetic Resonance, 9:299-336, 1997

[6] WS. Price. Pulsed-Field Gradient Nuclear Magnetic Resonance as a Tool for Studying Translational Diffusion: Part 1. Basic Theory. Concepts of Magnetic Resonance, 9:299-336, 1997

[7] EO. Stejskal, JE. Tanner . Spin diffusion measurements - spin echoes in presence of a time-dependent field gradient. *J Chem Phys* 42:288–292, 1965

[9]M.A. Horsefield and D.K. Jones. Applications of diffusion-weighted and diffusion tensor MRI to white matter disease – a review. *NMR in Biomedicine*, 15(7-8):570-577, 2002

[10] Y. Assaf, P.J. Basser. Composite hindered and restricted model of diffusion (CHARMED) MR imaging of the human brain. NeuroImage 27:48-58, 2005

[11]CA. Clark and D. Le Bihan. Water diffusion compartmentation and anisotropy at high b values in the human brain. *Magnetic Resonance in Medicine*, 44(6):852-859, 2001.

[12] CA. Clark, M. Hedehus, and ME. Mosely. In Vivo Mapping of the Fast and Slow Diffusion Tensors in Human Brain. *Magnetic Resonance in Medicine*, 47:623-628, 2002.

[13]Y. Assaf, J. Chapman, D. Ben-Bashat, T. Hendler, Y. Segev, A. D. Korczyn, M. Graif and Y. Cohen. White matter changes in multiple sclerosis: correlation of q-space diffusion MRI and [1]H MRS. *Magnetic Resonance Imaging*, 23(6):703-710, July 2005.

[14] C-P Lin, V. J. Wedeen, J-H Chen, C. Yao and W-Y Tseng. Validation of diffusion spectrum magnetic resonance imaging with manganese-enhanced rat optic tracts and ex vivo phantoms. *NeuroImage* 19:482-495, 2003.

[15] O. Brihuega-Moreno, F. P. Heese, C. Tejos and L. D. Hall. Effects of, and corrections for, Cross-Term Interactions in Q-space MRI. *Magnetic Resonance in Medicine*, 51:1048-1054, 2004.

[16] Y. Assaf, D.Ben-Bashat, J. Chapman, S. Peled, I. E. Biton, M. Kafri, Y. Segev, T. Hendler, A.D. Korczyn, M. Griaf and Y. Cohen. High b-Value q-Space Analyzed Diffusion-Weighted MRI: Applications to Multiple Sclerosis. *Magnetic Resonance in Medicine*, 47:115-129, 2002.

[17]P. P. Mitra and B. I. Halperin. Effects of Finite Gradient-Pulse Widths in Pulsed-Field-Gradient Diffusion Measurements. Journals of Magnetic Resonance, Series A, 113(1):94-101, 1995.

[18] E. K. Joeng, S. E. Kim, D. L. Parker. High-resolution diffusion-weighted 3D MRI, using diffusion-weighted driven equilibrium (DW-DE) and multishot segmented 3D-SSFP without navigator echoes. Magnetic Resonance in Medicine 50:821-829, 2003.

[19] J. Lätt, M. Nilsson, A. Rydhög, R. Wirestam, F. Ståhlberg and S. Brockstedt. Effects of restricted diffusion in a biological phantom: A q-space diffusion MRI study of asparagus stems at a 3T clinical scanner. Magn Reson Mater Phy DOI : 10.1007/s10334-007-0085-z.

[20] S. Boujraf, R. Luypaert, H. Eisendrath, M. Osteaux. Echo planar magnetic resonance imaging of anisotropic diffusion in asparagus stems. Magnetic resonance Materials in Physics, Biology and Medicine 13:82-90, 2001

[21]E. E. Sigmund and Y.-Q. Song. Multiple echo diffusion tensor acquisition technique. Magnetic Resonance Imaging 24:7-18, 2006

[22] Wikipedia. Parenchyma, the free encyclopedia, 2006. [Online; access 11-Dec-2006]

[23] Wikipedia. Vascular bundle, the free encyclopedia, 2006. [Online; access 11-Dec-2006]

[24] Y. Assaf, R. Z. Freidlin, G. Rohde, P J. Basser. New Modeling and Experimental Framework to Characterize Hindered and Restricted Water Diffusion in Brain White Matter. MRM 52:965-978 (2004)

[25] A. Bibic. Denoicing of Complex MRI Data by Wiener-like Filtering in the Wavelet Domain: Application to High b-value Diffusion Weighted Imaging. Degree project 20 credits in medical radiation physics. Spring 2005 Departent of Medical Physics, Lund University.